Available online at www.sciencedirect.com
SCIENCE DIRECT®
Pergamon
Acta Materialia 51 (2003) 4379–4394
Acta MATERIALIA
www.actamat-journals.com

Bonding mechanism in cold gas spraying

Hamid Assadi [a], Frank Gärtner [b,*], Thorsten Stoltenhoff [b], Heinrich Kreye [b]

[a] *Department of Materials Engineering, Tarbiat Modarres University, P.O. Box 14115-143, Tehran, Iran*
[b] *Department of Mechanical Engineering, University of the Federal Armed Forces Hamburg, Hamburg D-22043 Germany*

Received 31 July 2002; accepted 5 May 2003

Abstract

Cold gas spraying is a relatively new coating process by which coatings can be produced without significant heating of the sprayed powder. In contrast to the well-known thermal spray processes such as flame, arc, and plasma spraying, in cold spraying there is no melting of particles prior to impact on the substrate. The adhesion of particles in this process is due solely to their kinetic energy upon impact. Experimental investigations show that successful bonding is achieved only above a critical particle velocity, whose value depends on the temperature and the thermomechanical properties of the sprayed material. This paper supplies a hypothesis for the bonding of particles in cold gas spraying, by making use of numerical modelling of the deformation during particle impact. The results of modelling are assessed with respect to the experimentally evaluated critical velocities, impact morphologies and strengths of coatings. The analysis demonstrates that bonding can be attributed to adiabatic shear instabilities which occur at the particle surface at or beyond the critical velocity. On the basis of this criterion, critical velocities can be predicted and used to optimise process parameters for various materials.

Keywords: Cold gas spraying; Particle impact; Modelling; Bonding; Adiabatic shear instability

1. Introduction

In thermal spray processes, the quality of coatings is influenced by both, the degree of melting and the velocity of the sprayed particles. In high velocity oxy-fuel (HVOF) spraying, for instance, a significant proportion of particles is still solid as they impinge the substrate [1–4]. The formation of dense and tightly bonded coatings in spraying processes can thus be attributed not only to the thermal energy but also to the kinetic energy of particles upon impact. In cold gas spraying, very high particle velocities are obtained by the acceleration of an expanding gas stream to velocities in the range of 500–1200 m/s in a converging diverging DeLaval type nozzle [5–10]. In this process, the gas is heated, without using combustion, only to increase the gas and particle velocity and to facilitate the deformation of particles upon impact. The gas and particle temperatures remain well below the melting temperature of the spray material. The particles are therefore in the solid state as they hit the substrate, and formation of coatings occurs only due

* Corresponding author. Tel.: +49-40-6541-2887; fax: +49-40-6541-2006.
E-mail address: frank.gaertner@unibw-hamburg.de (F. Gärtner).

1359-6454/03/$30.00
doi:10.1016/S1359-6454(03)00274-X

to the kinetic energy of the particles. Cold gas spraying is therefore particularly suitable for spraying and coating materials which are sensitive to heat or oxidation and would transform or react in conventional spraying processes. It has been demonstrated that cold gas sprayed coatings of oxidation sensitive materials such as Ti or MCrAlY show similar, or only slightly higher oxygen contents than their respective powder feedstock [11,12].

The bonding of particles in cold gas spraying is presumed to be the result of extensive plastic deformation and related phenomena at the interface [9,13–15]. The bonding mechanisms in cold gas spraying can thus be compared to those in processes such as explosive cladding or shock wave powder compaction. These latter processes have been explored widely with respect to mechanisms of bonding as well as to possible applications [16–18]. In explosive cladding, successful bonding occurs within a certain range of impact angles, impact velocities and materials properties, and it is often manifested by the formation of an out-flowing jet of material at the contact zone [19]. Within a distance of a few millimetres from the interface, there is a sequence of regions with severe deformation, highly elongated grains, recrystallised grains, and sometimes resolidified microstructures, though melting and resolidification are often limited to a thickness of less than a micrometer at the interface [20]. In explosive powder compaction, dense solids of materials ranging from metals such as aluminium, steels and nickel based superalloys, to ceramics can be produced by appropriate selection of shock pressure and duration [21–26]. In analogy with explosive cladding, successful bonding in powder compaction, also, has been related to critical conditions for extensive plastic deformation at the particle/particle interface [23,27]. Microstructural studies of compacted powder of some nickel-base alloys, indicate the formation of amorphous phases due to rapid cooling [28]. There is also evidence for the formation of a fast travelling jet at the particle/particle interface in powder compaction studies [18,22,25].

Despite the existing analogies among these processes, it has not yet become clear as to what extent the concepts of explosive cladding or shock wave powder compaction can be applied to cold gas spraying. There have been a number of studies focusing on the relationships between the measured deposition efficiencies and the particle velocities as evaluated by semi-empirical methods and numerical modelling [8,12,29,30]. These investigations propose the existence of a critical particle velocity for successful bonding, whose value depends most significantly on the thermomechanical properties of the spray and also the substrate materials. Below this velocity, impacting particles would only cause densification and abrasion of the substrate, in a way similar to that in grit blasting or shot peening. Moreover, scanning and transmission electron microscopy of cold gas sprayed coatings show features on a very localised scale which are comparable to those observed in explosive cladding or explosive powder compaction [13–15]. Previous studies also include numerical analyses of particle impact in cold gas spraying, providing a description of the deformation pattern and temperature distribution in the particle and substrate [13].

The aim of this paper is to explore mechanisms of bonding and to explain the observed critical velocities in cold gas spraying, by means of numerical analysis of particle impact. The present study includes a description of the mechanical state and thermal history of the individual particles during impact. The results of the analyses are then discussed in view of possible correlations with the measured critical velocities and other experimental observations. In this way, possible criteria for particle bonding in cold gas spraying are assessed. Based on these criteria, correlations between the critical velocity and key parameters of the process and material properties are evaluated. These correlations provide a better understanding of the cold spray process and contribute to its optimisation.

2. Methods

2.1. The cold gas spraying process

Principles of cold gas spraying and the experimental set-up for the preparation of coatings have been described elsewhere [12] and are summarised

schematically in Fig. 1. Process parameters such as gas type, pressure and temperature were optimised to yield maximum deposition efficiency and minimal porosity, with respect to size distribution, morphology and oxygen content of the particles of the spraying powder. In case of cold gas spraying of copper, nitrogen or helium, preheated to 320 °C, were used as process gases. To study the impact of single particles on the substrate, less than a monolayer of particles was deposited by wipe tests, in which the substrate was moved rapidly perpendicular to the stream of particles.

2.2. Semi-empirical determination of critical velocities

Details of the procedure used to determine the critical velocities are reported in detail in [12]. Initially, particle velocity distributions for a given set of processing conditions were calculated by using computational fluid dynamics (CFD). This was then verified against the corresponding mean velocity as measured by laser doppler anemometry (LDA). Subsequently, the velocity distribution was combined with the measured deposition efficiency and the particle size distribution, to give the size and velocity of the largest particle which would bond successfully to the substrate. The corresponding calculated velocity for this largest, and hence slowest, bonded particle was taken as the critical velocity for bonding.

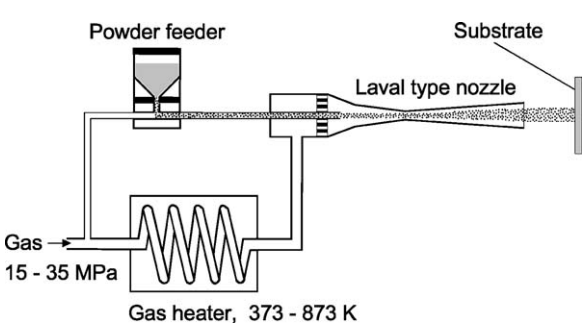

Fig. 1. Schematic diagram of the set-up used for cold gas spraying in the present study. The spray gun is mounted on a robot system to give the required raster speed.

2.3. Microstructural investigations

Impact morphologies of copper particles on copper substrates were studied by scanning electron microscopy. Cross sections of the coated samples were prepared to study the particle/substrate interfaces. In case of wipe tests, the samples were also studied from a top or a perspective view.

2.4. Measurement of strength

The adhesive strength of cold gas sprayed coatings was determined according to the European standard EN 582. Top surfaces of cylindrical samples were coated and then glued to respective counter-bodies of the same size. The specimens were then exposed to tensile forces along their axes in a tensile-testing machine. The ruptured specimens were screened to determine the location of failure, which could be at the interfaces between (i) coating and substrate, (ii) neighbouring particles within the coating, or (iii) coating and glue.

2.5. Modelling of deformation

Deformation of the particles upon impact was analysed by using the finite element program ABAQUS/Explicit version 6.2-1 [31]. The analysis accounted for strain hardening, strain-rate hardening, thermal softening, and heating due to frictional, plastic and viscous dissipation. In most cases, the heating was assumed to be adiabatic, i.e., heat transfer was not considered. In modelling of high strain rate phenomena, the validity of this assumption can be assessed with respect to the value of the dimensionless parameter $x^2/D_{th}t$, in which x is a characteristic system dimension, D_{th} is thermal diffusivity and t is the process time [32]. A value of $x^2/D_{th}t$ equal or above unity is considered to justify the assumption of adiabatic heating. The value of this parameter can be shown to be well above unity for the case of particle impact in cold gas spraying, by taking typical values of 10^{-6} m^2/s for D_{th}, 10 ns for t and 10^{-6} m for the element size in a particle of 10^{-5} m in diameter. It should nevertheless be noted that the above argument is based on the solution of the diffusive heat equation. At very small length scales, heat conduc-

tion would be dominated by a wave propagation mechanism rather than by diffusion [33,34]. This implies that with decreasing particle size, the speed of heat propagation would approach that of plastic waves, and would in any case be limited by the speed of sound in the particle. In other words, for high speed impacts of much smaller particles, heat conduction could be even slower than what is predicted by the diffusive heat equation. Therefore, it could still be reasonable to assume adiabatic heating even for the impact of very small particles for which $x^2/D_{th}t$ would fall below unity. It has also been suggested that the dissipation of kinetic energy into heat is strain rate dependent, i.e., the fraction of plastic work dissipated into heat would be larger for higher strain rates [35]. This would further support the assumption of adiabatic heating in cold gas sprayed particles. Nevertheless, in order to leave a margin for heat conduction and stored energy, only 90% of the kinetic energy was assumed to dissipate into heat.

Modelling of particle impact was performed initially for copper as a reference material. The choice of copper was made in view of both feasibility of coating formation by cold gas spraying and availability of relevant material data in the literature (e.g., [36–39]). In most cases, the plastic response of copper was assumed to comply with the Johnson–Cook plasticity model as follows

$$\sigma = [A + B\varepsilon^n][1 + C\ln\dot{\varepsilon}^*][1-T^{*m}] \quad (1)$$

where σ is the flow stress, ε is the equivalent plastic strain, $\dot{\varepsilon}^*$ is the equivalent plastic strain rate normalised with respect to a reference strain rate, and $T^{*m} = (T-T_{ref})/(T_m-T_{ref})$ in which T_{ref} is the temperature above which thermal softening can occur, and T_m is the melting temperature. The constants A, B, n, and m are taken from [36] and are listed in Table 1. The elastic response of the material was assumed to follow a linear elasticity model. This assumption was found to be adequate for most cases of simulations, especially for low and moderate particle impact velocities. A linear Mie–Gruneisen equation of state (EOS) was employed alternatively for comparison with the linear elasticity model. In ABAQUS, this has the following form

$$p-p_H = \rho\Gamma(E_m-E_H) \quad (2)$$

Table 1
Material data for copper

Properties	Parameter	Unit	Value
General	Density	kg/m^3	8960
	Specific heat	J/kg K	383
	Melting temperature	K	1356
	Thermal expansion	1/K	5×10^{-5}
Elastic	Young's modulus	GPa	124
	Poison's ratio	–	0.34
Plastic (Johnson–Cook model)	A	MPa	90
	B	MPa	292
	n	–	0.31
	C	–	0.025
	m	–	1.09
	Reference temperature	K	298
	Reference strain rate	1/s	1

where p_H and E_H are the Hugoniot pressure and specific energy, respectively, and Γ is the Gruniesen ratio [31]. The material parameters required for these calculations were taken from [37].

Analyses were performed by using axisymmetric, and three-dimensional models of particle impacts, with various combinations of calculation settings concerning element type, initial and adaptive meshing, contact interaction, etc. For axisymmetric analyses, 4-node elements with hourglass control were used. Initial meshing was performed by using the built-in free-meshing algorithm of ABAQUS/CAE. The initial element size varied from region to region, but for most cases of analysis it was kept about 1/50 of the particle size near the contact area. Adaptive meshing was used initially to cope with large deformations near the contact surfaces. This was done with the objective of preserving initial mesh grading, combined with the built-in second-order advection and half-index shift momentum advection methods of ABAQUS/Explicit [31]. Nevertheless, for moderate and high particle impact velocities, frequent remeshing resulted in non-conserving energy variation of the output set, and in unphysical shape of the out-flowing jet of material at the interface. To alleviate this problem, remeshing was performed only as frequent as necessary; i.e., in most cases the frequency of remeshing was kept lower than one in every 50 increments. Three-dimensional

analyses were performed without adaptive meshing, by using 4-node linear tetrahedron elements. Both types of analysis were performed mainly for identical particle and substrate materials and for particle sizes in the range from 5 to 100 μm. The initial impact velocity was taken as the prime input variable. The deformation pattern and the key field variables were examined generally throughout the particle and substrate, but also particularly along various paths within the particle. The temporal evolution of these variables at specified locations at the surface were also studied. Fig. 2 shows an example of the initial configuration, the paths, and the boundary conditions assumed for an axisymmetric analysis. The substrate has no degree of freedom at the bottom, and can only slide in the vertical directions at the lateral edges.

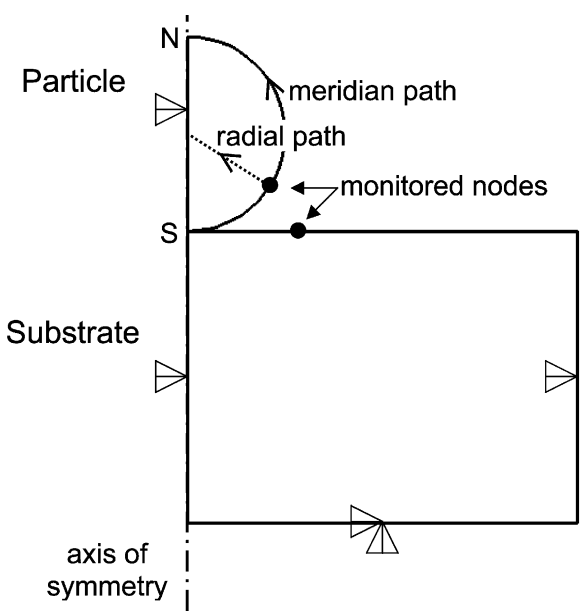

Fig. 2. Initial configuration and boundary conditions for an axisymmetric model. The substrate is fixed at the bottom, and horizontal displacement is not allowed at the axis of symmetry and at the outer edge. The profiles of field variables are investigated along meridian and radial paths as shown in the figure. The development of these variables with time is studied at selected nodes at the surface, which are subject to highest amount of deformation.

3. Experimental results

3.1. Critical velocities

By using the method described in Section 2.2, a critical velocity of 570 m/s was obtained for inert-gas-atomised 99.8% copper powder with particle size ranging from 5 to 22 μm. The critical velocity was determined to be 660 m/s for inert-gas-atomised 99.93% aluminium powder with particle size below 45 μm. These values are consistent with those reported previously by other researchers [5,8]. The mean particle velocities, as measured by LDA, agreed well with the calculated mean velocities. However, this experimental method could not give an unambiguous correlation between particle sizes and velocities

3.2. Deformation morphologies

Fig. 3 shows micrographs of impacted particles of copper on a copper substrate. The impact velo-

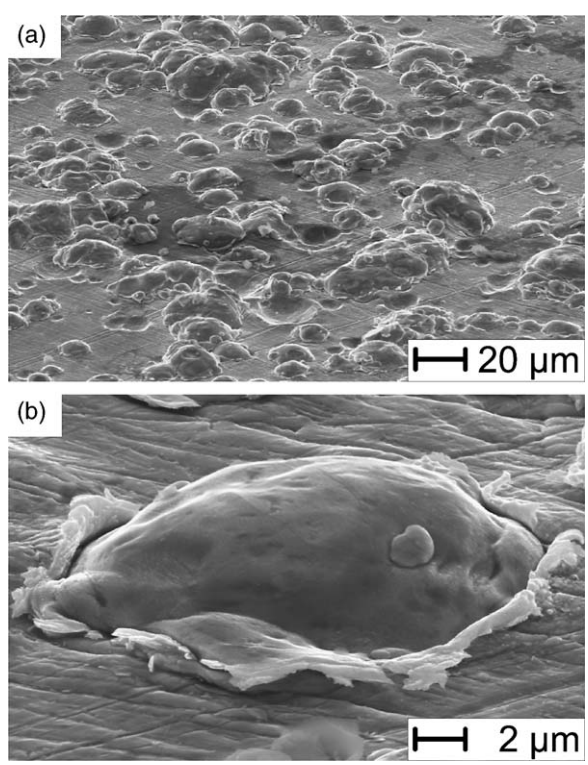

Fig. 3. Scanning electron micrographs (secondary electron mode) of wipe test samples of copper particles on a copper substrate, showing (a) an overview and (b) a close-up image.

cities were calculated to be in the range from 550 to 670 m/s for particle sizes between 5 and 25 μm. Overviews at low magnifications demonstrate that more than 80% of the impacting particles adhere to the substrate (Fig. 3a). The close-up view in Fig. 3b illustrates a bonded particle which is accompanied by the formation of a ring of a jet-type morphology around the impact zone. The micrographs also show that the deformation of secondary particles is influenced by the morphology created by primary impacts. The non-adhering particles leave craters in the substrate without any indication of a jet-type feature. The height and diameter of the adhering particles in a N_2-sprayed sample were determined from cross-section micrographs. The mean flattening ratio, defined as the ratio of the diameter of splat to that of a spherical particle of the same volume, was calculated to be 1.31 for this sample. It should be noted that this value is inevitably associated with an error, which arises from the underestimation of the particle volume. This is due to the fact that cross sections do not normally pass through the centre of splats. For a He-sprayed sample a larger flattening ratio was obtained by, alternatively, comparing the diameters of the adhering particles—as obtained from top-view SEM micrographs—to the particle size distribution of the initial powder feedstock—as determined by sieving analysis. More results will be given and compared to the results of modelling later in this paper.

Fig. 4 shows a cross-section of a 1 mm thick copper coating. The particles appear to be tightly bonded throughout their entire surfaces and there is only a very small amount of porosity within the coating. The micrograph reveals jet-type features and elongated morphologies.

3.3. Strength of coatings

The strength tests of cold gas sprayed coatings of copper on copper or steel substrates reveal that in most cases failure occurs at the coating/substrate interface. For the employed spraying conditions, the adhesive strengths were typically in the range from 30 to 40 MPa. Higher values were obtained with higher gas and particle velocities. This means that the strength of cold gas sprayed coatings of copper can be as low as 20% of the yield strength of work hardened copper, when typical velocities for building up dense coatings are used. In contrast to the tight appearance of the coatings (Fig. 4), the relatively low strength of these coatings suggests imperfect bonding at the particle/particle interfaces.

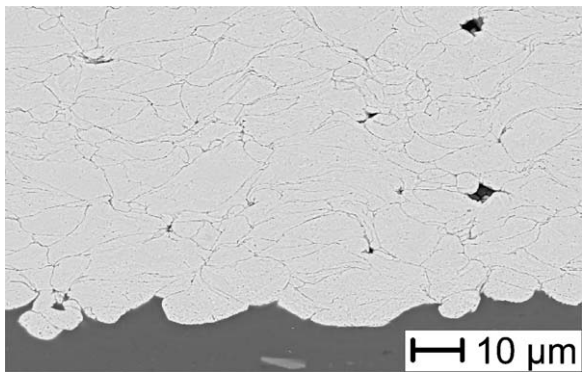

Fig. 4. Scanning electron micrographs (back-scattering mode) of a cross-section of a cold gas sprayed copper coating on an aluminium substrate. The sample was etched to reveal the particle/particle boundaries. The particles appear to be tightly bonded, and there is very little porosity within the coating.

4. Results of numerical modelling

4.1. General aspects of particle impact

Fig. 5 shows the deformation pattern in a copper particle during impact onto a flat copper substrate, for two initial velocities of 500 and 600 m/s. The particles and substrates are initially at room temperature. The contours indicate temperature and the arrows represent the magnitude of velocity at the respective surfaces. The figure shows very localised heating near the particle/substrate interface for both impact velocities, though this is more severe for the higher velocity impact. The figure also shows the formation of a jet-type flow of material at the interface at an early stage of impact. To verify parameter settings, flattening ratios obtained by modelling were compared to results from investigating cross sections of single impacts. As shown in Fig. 6, the modelled flattening ratio of Cu-particles impacting on Cu-substrates, is slightly

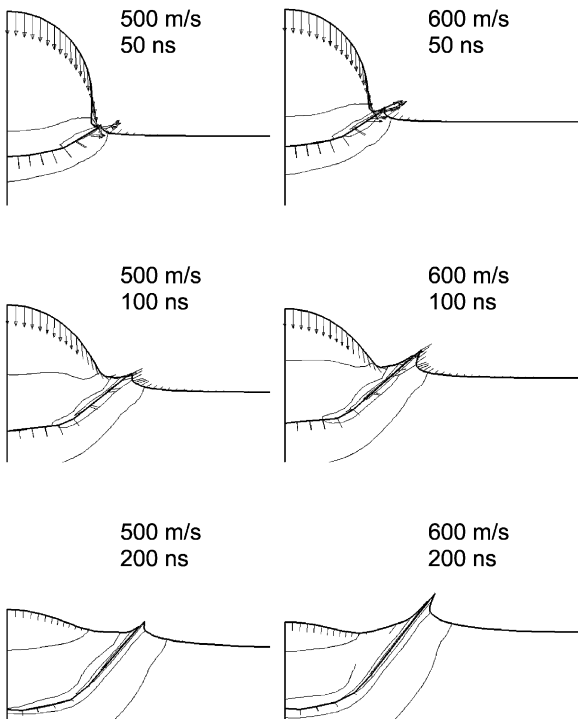

Fig. 5. Simulated impact of a copper particle on a copper substrate, for the initial velocities of 500 and 600 m/s. The arrows represent the velocities of nodes at the respective surfaces of particle and substrate, and the contours indicate temperature distribution.

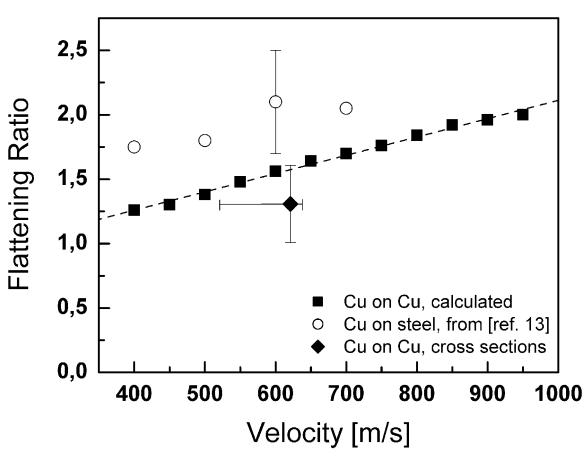

Fig. 6. Flattening ratios as obtained from impact modelling and experimental investigations. Cross-sections are from a nitrogen-sprayed copper powder. The data for copper particles on steel are taken from Ref. [13].

increasing with velocity. Profilometric investigations of single impacts of Cu-particles on steel show larger flattening ratios which can be attributed to the higher hardness of the substrate material [13]. For N_2-sprayed powder, a mean particle velocity can be calculated by CFD. For similar velocities, the experimental flattening ratio is slightly smaller than that obtained by modelling. This difference can be attributed to the underestimation of particle diameters in cross sections and therefore the overestimation of impact velocities. A better statistical basis can be obtained by comparing diameters of adhering particles in top view with that of the initial powder feedstock (Fig. 7). For the different sizes of the initial powder population as calculated on the basis of sieving analyses, particle velocities were determined by CFD. With the velocity-dependent flattening ratio obtained from impact modelling, the top view size distribution of impacted particles of that particular powder can be calculated. As shown in Fig. 7, calculated and measured top view size distributions match reasonably. The slightly larger size of the experimentally determined population can be attributed to the fact that over-hanging material or jets contribute to an overestimation of splat sizes as obtained by SEM-analysis.

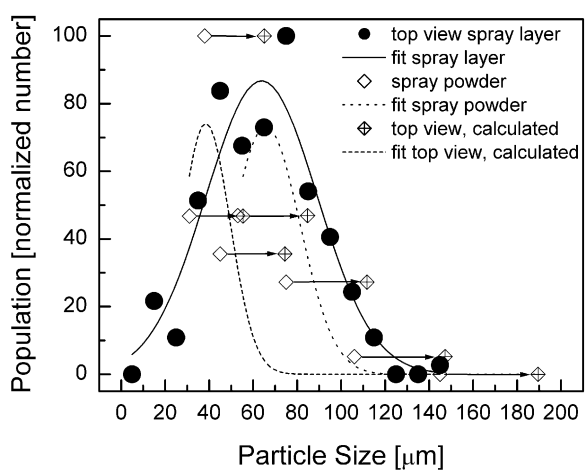

Fig. 7. Size distributions of a copper powder, before and after spraying with helium. The splat diameters are also calculated based on the corresponding initial sizes and the CFD/impact modelling. As a guide for the eye, Gaussian fits to the respective populations are indicated.

As shown in Fig. 8, the velocity of a node at the particle surface can reach twice as much the impact velocity. The figure also shows that the flow of substrate material can take place at a speed greater than the initial impact velocity. This rapid increase of velocity at the particle and substrate surfaces can be considered as a measure to indicate jet formation.

In order to obtain a better understanding of the localisation of plastic deformation, the strain and stress profiles along a radial path (as indicated in Fig. 2) can be examined. Fig. 9a shows an example of such a profile for a 10 μm particle, 5 ns after the beginning of the impact, for two initial velocities of 300 and 900 m/s. The corresponding variation of the equivalent (von Mises) flow stress along the same path is shown in Fig. 9b. For the impact velocity of 300 m/s, there is a monotonic increase in flow stress by approaching the interface. This is a result of hardening effects due to high strains and strain rates at the interface. The high plastic strain at the interface can on the other hand result in softening due to adiabatic heating. This softening effect can dominate against the hardening effects at higher velocities and lead to an adiabatic shear instability at the interface. This effect is observed clearly for an impact velocity of 900 m/s. For this velocity, despite the high magnitude of plastic strain at the interface, the shear strength of material falls to values near zero due to dominance of thermal softening over hardening effects.

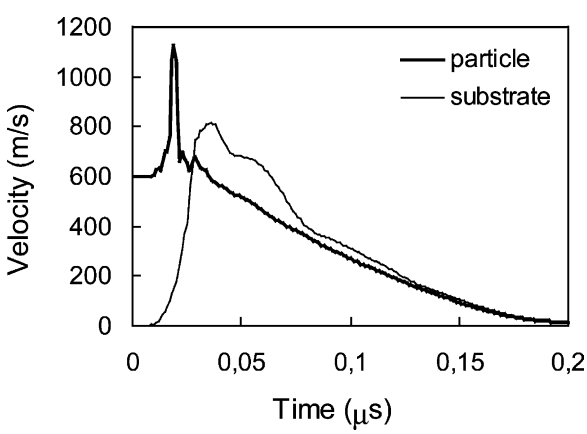

Fig. 8. Calculated velocity magnitudes at the critical nodes (as indicated in Fig. 2) on the respective surfaces of particle and substrate. The velocity of the monitored nodes at the particle and substrate surfaces exceeds the initial particle velocity, for a short period after the initial contact.

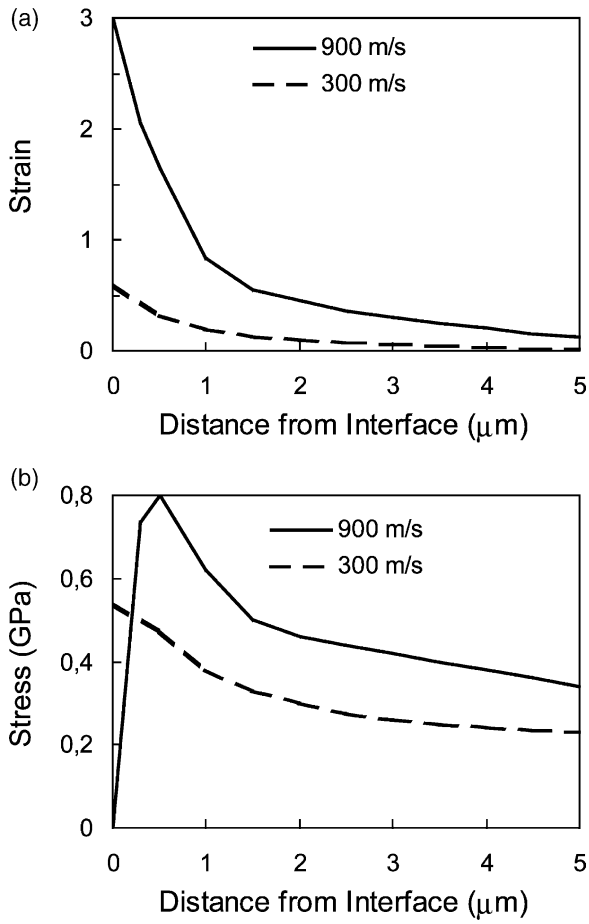

Fig. 9. Calculated profiles of (a) plastic strain and (b) flow stress along the radial path (as indicated in Fig. 2) for impact velocities of 300 and 900 m/s. Both, strain and stress increase monotonically by approaching the interface for the smaller impact velocity. For the higher velocity, however, the shear stress falls to zero at the interface, indicating an adiabatic shear instability.

4.2. Condition for adiabatic shear instability

Thermal softening and adiabatic shear instability at the interface could play a significant role in the set of microscopic processes leading to successful bonding of particles in cold gas spraying. The results of the above analyses (Fig. 9) outline a win-

dow of conditions for this to take place. The next step would be to obtain a more precise evaluation of the particle impact velocity corresponding to the threshold of adiabatic shear instability. For such evaluations, it should be considered that the variation of the degree of deformation with distance is strongly non-linear near the particle/substrate interface. On the other hand, the calculated field variables, such as strain or temperature, would only represent the average respective values within a particular element. For an element at the interface, where the plastic deformation is highly localised, such average values may therefore deviate substantially from the real values at the interface. This is so because the element size scales with the shortest distance from the interface. A larger element size would consequently result in a larger deviation. This causes a part of the results from modelling to depend strongly on the element size. Fig. 10 shows the calculated maximum temperature at the interface for various element sizes and impact velocities. As indicated in the figure, all calculated temperatures fall below melting temperature of copper. However, these vary with the element size, in the sense that higher temperatures are obtained when a finer mesh is chosen. As an initial solution to filter out the element size effect, the "real" maximum temperature has been worked out by linear extrapolation to "zero element size". This real

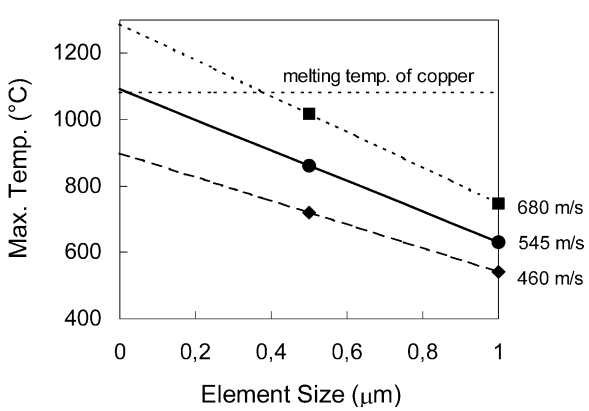

Fig. 10. Calculated maximum temperatures for various element sizes and impact velocities, showing an increase of temperature with decreasing element size. Extrapolation of maximum temperature to zero element size coincides with the melting temperature of copper for an impact velocity of 545 m/s.

maximum temperature coincides with the melting temperature of copper for an impact velocity of 545 m/s. In a first approximation, therefore, this value could be taken as corresponding to the threshold of an adiabatic instability.

In subsequent analyses, the problem of element size dependence was alleviated by refining the mesh structure near the interface, down to element sizes of about 0.2 μm. Fig. 11 shows the development of plastic strain, temperature and flow stress in a so-called critical element at the particle surface which undergoes the highest amount of deformation within the particle. As shown in Fig. 11a, the plastic strain increases very rapidly at a rate of up to 0.5×10^9 s^{-1}, before reaching its final value of about 4 for three velocities of 450, 500 and 550 m/s. For the velocity of 580 m/s the trend is nevertheless different, showing a further increase of strain up to a final value of about 10. The increase of strain at this velocity could be the result of a change in mechanism from plastic to viscous flow. This will be discussed below in more detail. The temporal development of temperature in the critical element (Fig. 11b) is similar to that of strain, but with small differences which are due to differences in frictional and viscous dissipations. The heating rates for all impact velocities are around 10^9 K/s in the first step. For the impact velocity of 580 m/s, the temperature approaches the melting temperature of copper, whereas in other cases it remains well below it. Fig. 11c shows the temporal development of the equivalent stress. For lower or medium velocities of up to 550 m/s, there is a drop in stress after 0.05 μs, which can be attributed to the loading conditions from the substrate. But for the impact velocity of 580 m/s, there is a significant change in trend of temporal development of stress at an earlier time of 0.03 μs. Beyond this time, the stress variation is accompanied with large fluctuations, as well as a decrease in the overall value. The change in stress variation coincides with the increase of strain and temperature in the critical element, as shown in Fig. 11. The fluctuations in temporal development of stress at a high velocity (580 m/s) could be explained with respect to a change in deformation mechanism from plastic to viscous flow. Near the conditions for thermal softening, the resistance of material to shear flow

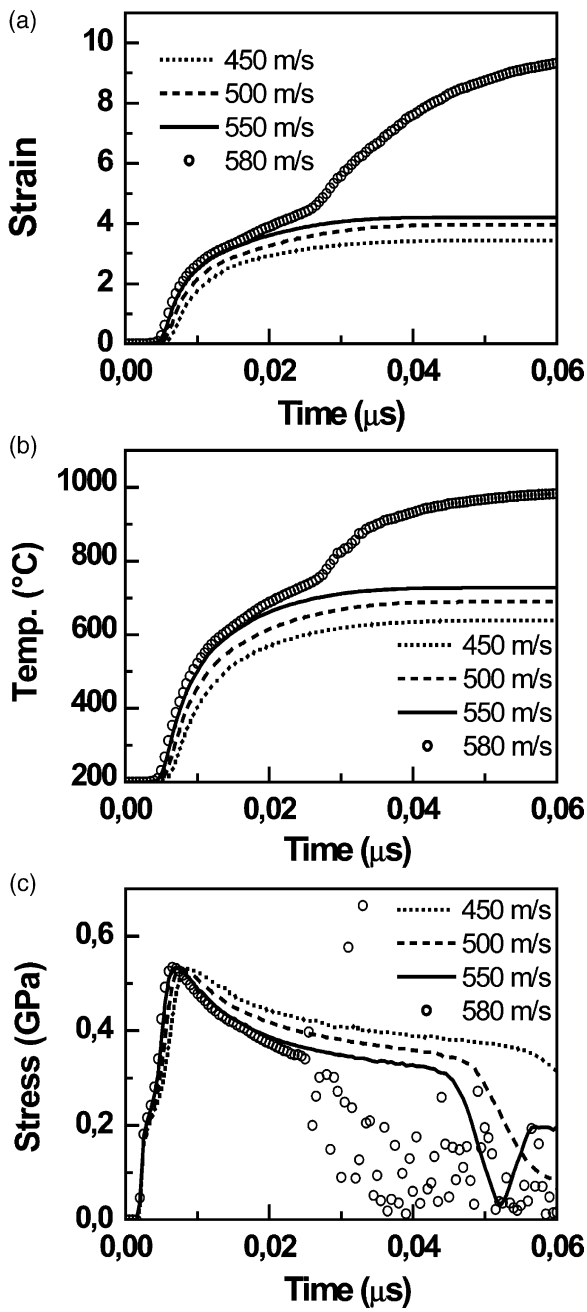

Fig. 11. Calculated temporal development of (a) plastic strain (b) temperature and (c) flow stress at the critical node of a sprayed particle (as indicated in Fig. 2) for various impact velocities. There is a change in trend of variation of these variables with time, as the initial particle velocity is increased from 550 to 580 m/s, indicating a shear instability.

is generally low. This means that by approaching the melting temperature, the material loses its shear strength and undergoes excessive deformation for any amount of imposed shear stress. On the other hand, this excessive deformation would create a viscous-type resistance which would hinder further deformation, particularly under high pressure. In the present analysis, this effect will be due to the increase in the second term of the Johnson-Cook model which accounts for strain-rate hardening. Additionally, the loading conditions at the particle surface may change as a result of changes in strength, thus contributing to further fluctuations in stress. A successive interplay of these three effects results in large-amplitude fluctuations as observed in the stress plots. It should be noted that these fluctuations may not accurately represent the real state of stress at the interface, as they are also influenced by the selected calculations parameters such as mesh size. However, they are still important features in the results of modelling, as they signify the beginning of a shear instability. The overall level of stress decreases with time because of accumulating viscous dissipation which results in further increase of temperature and decrease of strength. The rapid changes of field variables such as strain, temperature and stress for a critical element show that transitions from plastic flow to viscous flow can occur within a narrow range of velocity between 550 and 580 m/s. Taking into account the effect of element size, which would lead to an overestimation of the velocity for adiabatic shear instability, the latter result can be considered to be in agreement with the transition velocity of 545 m/s as estimated earlier (Fig. 10).

4.3. Non-uniformities at the particle–substrate interface

The interpretation of the results of modelling has so far been based on the development of field variables at selected nodes at the interface. In order to obtain a better insight to the bonding mechanism in cold gas spraying, several other factors have to be taken into account. It would for instance be of prime importance to know not only the threshold of transition to thermal softening but also the extent of plastic deformation and viscous flow at

the interface. This can be illustrated by plotting the field variables such as the equivalent plastic strain along a meridian path (Fig. 2) on the particle surface. Fig. 12 shows examples of such plots corresponding to various times and impact velocities. The plots also indicate that the contact area between particle and substrate grows with the progress of impact and with increasing the impact velocity. For short and medium times after the initial contact, there is an increase of plastic strain with distance from the south pole up to the edge of the contact zone. The increase of plastic strain with time at specific distances along the path is however small. The condition for shear instability is manifested here by a sharp rise in the plastic strain near the edge of the contact zone for the impact velocity of 580 m/s. The temperature distribution along a meridian path is similar to that of strain, though this has not been shown here. Again, the start of adiabatic instability is manifested by a sharp increase of temperature to values near the melting temperature of copper. The only difference is that the rise in temperature near shear instability conditions is less pronounced than that in strain. Similarly, this could be attributed to the change from plastic to viscous dissipation of kinetic energy into heat.

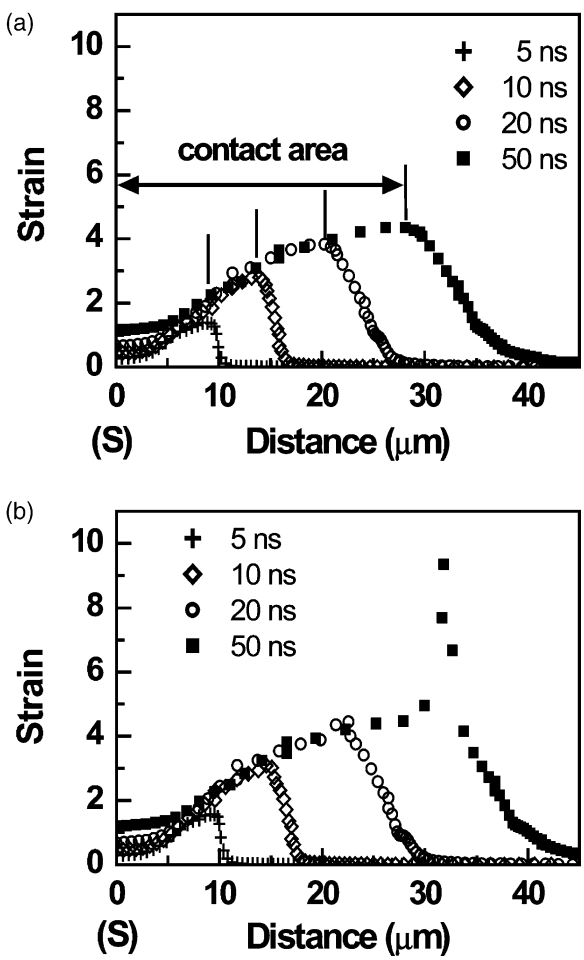

Fig. 12. Calculated profile of plastic strain along the meridian path on the particle surface, for various times after impact, for impact velocity of (a) 550 and (b) 580 m/s. The limit of the contact zone is indicated by vertical lines on plot (a). The strain increases always monotonically from the initial point of contact (south pole) up to a maximum at this limit. The extent of region which undergoes adiabatic shear instability (b) is limited only to a small fraction of the overall contact area.

4.4. Three-dimensional simulation

Axisymmetric models can be applied only to perpendicular impact of a single particle. In order to simulate interaction of particles during deposition, three-dimensional models should be used. Fig. 13 shows the result of a three-dimensional simulation for the overlapping impact of two copper particles of 5 μm diameter on a copper substrate. With respect to realistic impact conditions, initial velocities and temperatures were assumed to be 600 m/s and 200 °C, respectively. The initial distance between the two particles allows embedding of the first particle before the second particle hits the substrate (Fig. 13a). The formation of a jet-type ring of material around the impact zone is evident for both particles (Fig. 13b). However, the formation of the jet for the second particle is influenced by the change in morphology and properties of the underlying substrate as a result of the first impact (Fig. 13c). It should be noted that the relatively shorter time scale in three-dimensional analysis is due to the relatively smaller particle size as compared to those assumed in the axisymmetric models.

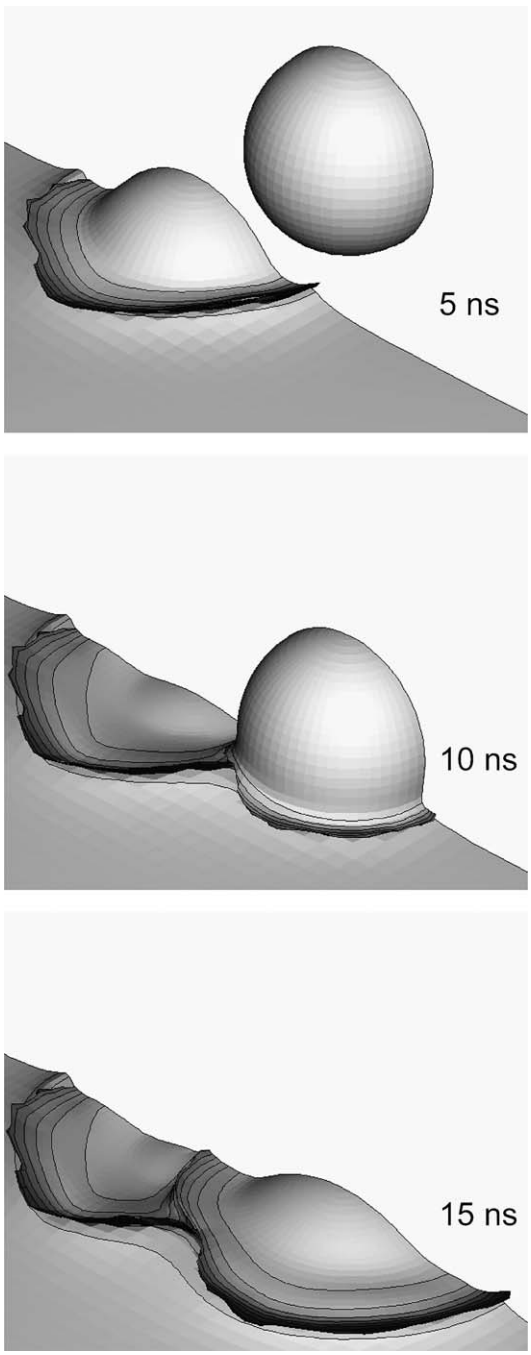

Fig. 13. Three-dimensional simulation of impact of two 5 μm particles with initial impact velocity of 600 m/s, at 5, 10, and 15 ns after the initial contact of the first particle with the substrate.

5. Discussion

5.1. Criteria for bonding

Bonding of particles in cold gas spraying can be influenced by various factors. These factors range from geometrical parameters such as the contact surface area, the depth and width of crater [13] to thermomechanical parameters such as plastic strain, flow stress, pressure, and temperature at the interface. These parameters are in turn influenced by the particle impact velocity. It would therefore be reasonable to assume that at velocities near the critical velocity, these parameters also would reach a critical value, or would show a change in trend in their variation with velocity. Postulation of any criteria for bonding would require determination of these critical values and conditions.

In explosive welding, the formation of a jet at the interface is often considered as a criterion for successful bonding [19]. This concept might seem to be applicable to the bonding of particles in cold gas spraying. Modelling of particle impact on a rigid substrate illustrates clearly the formation of a jet-type flow of material at the interface, but for impact on substrates of the same material, the jet is morphologically less prominent. In addition, depending on the calculation parameters such as the mesh size, a jet-type flow of material could occur over a wide range of impact velocities, thus making the criterion ineffective.

The results of the modelling show a change in trend of almost all key parameters near the particle interface with the beginning of adiabatic shear instability at the interface. Adiabatic shear instability is characteristically associated with high strain rate deformation. This phenomenon can be a cause for failure of mechanical components which are subject to high strain rate deformation. In cold spraying of copper, on the other hand, the velocity at the threshold of this instability is close to the experimentally evaluated critical velocity for copper [12]. This suggests that adiabatic shear instability could be the cause for bonding of particles in cold gas spraying. Based on this hypothesis, a criterion for bonding can be formulated by taking the critical velocity as being the same as that required for reaching adiabatic shear insta-

bility. This criterion allows the prediction of the critical velocity for a given material and particle temperature. However, it should be noted that the above criterion describes only one of several conditions required for bonding of particles. For instance, if the contact time is too short, or the applied tensile stress at the interface is too high, a particle may bounce back before the conditions for bonding are achieved. A particle impinging the substrate at an angle is an example of this case. In an angular impact, an additional temperature rise can occur at the interface due to frictional dissipation, which could promote shear instability. However, the tangential component of momentum of the particle in an angular impact would create a tensile force at the interface, which could be large enough to detach the particle from the substrate, despite the occurrence of shear instability at the interface.

5.2. Influence of process and materials parameters on critical velocities

By using the experimental method described previously, a critical velocity of 570 m/s was determined for cold gas spraying of a gas-atomised copper powder. This result is in good agreement with the transition velocities of 545 and 580 m/s as obtained from the modelling. To extend the results of the modelling to other materials and spraying conditions, the effect of various process parameters and material properties on the calculated critical velocity can be estimated by using the method described in Appendix A. This method can be used to estimate the effect of small changes in material and process parameters on the critical velocity. Examples of these parameters and their respective effects on the critical velocity are given in Table 2. The sign of the calculated derivatives indicates that the critical velocity increases with increasing yield stress and melting temperature, whereas it decreases with increasing density and particle temperature. For a typical range of material properties and process parameters, yield stress and melting temperature have a smaller effect on the critical velocity as compared to density and particle temperature. For instance, for each 1 g/cm^3 increase in density, there will be 14 m/s decrease in the critical velocity. The overall effect of these parameters can be summarised into the following simple formula

Table 2
Rate of change of critical velocity (m/s) with respect to material and process parameters

Property (a_i)	Unit	$\frac{\partial v_{cr}}{\partial a_i}$
Yield stress	MPa	0.1
Density	g/cm^3	−14
Elastic modulus	GPa	0.008
Melting temperature	K	0.08
Particle temperature	K	−0.4

$$v_{cr} = 667 - 14\rho + 0.08T_m + 0.1\sigma_u - 0.4T_i \quad (3)$$

where ρ is the density in g/cm^3, T_m is the melting temperature in °C, σ_u is the ultimate strength in MPa and T_i is the initial particle temperature in °C. By using respective values of density and melting temperature for aluminium, for instance, the critical velocity for this material can be estimated roughly to be about 620 m/s. Fig. 14 shows the critical velocities for a number of other materials which are estimated by using this approach for qualitative comparison. It should be stressed again

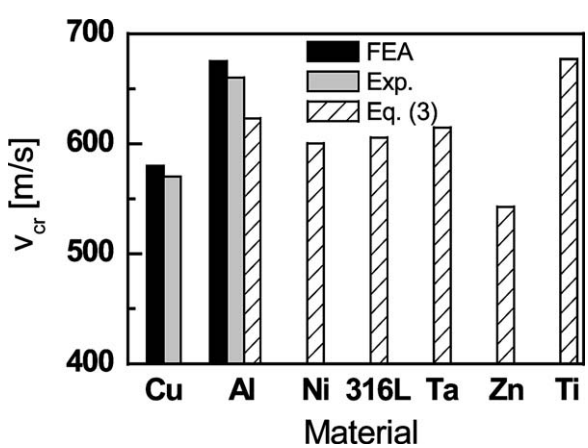

Fig. 14. The critical velocities of various materials, calculated (FEA) and measured (Exp.) for copper and aluminium, and estimated (Eq. (3)) for other materials by the approach described in Appendix A, by taking copper as reference material and considering only the differences in density and melting temperatures.

that the formula in Appendix A is valid only for small changes of involved parameters. For larger deviations from the reference condition, such as in the case of aluminium, the critical velocity should be calculated through a complete numerical analysis for the given set of spray parameters and materials properties. Performing such an analysis for aluminium, for instance, results in a critical velocity of 675 m/s, which is in a better agreement with the experimentally evaluated value of 660 m/s.

5.3. Deformation morphologies and the extent of bonded interfaces

The calculated deformation patterns as obtained by axisymmetric and three-dimensional modelling, are in reasonable agreement with the observed morphologies. This includes, in particular, the formation of a jet-type flow of material at the interface. There is also an agreement between the calculated and measured flattening ratios in this study. As shown in Fig. 7, the calculated and measured top view size distributions match also reasonably well. Differences between the results of modelling and experiments can be attributed partly to the errors arising in estimating flattening ratios from cross sections, and also in measuring top view diameters in the presence of jet-type features. Nevertheless, profilometric investigation of single impacts of copper particles on steel shows significantly larger flattening ratios [13]. This latter difference can be attributed to the difference in hardness of the substrate materials. The results of modelling also show that extensive plastic deformation at the critical velocity is confined to an outer region within the particle/substrate interface. This means that softening of the entire particle–substrate interface would require higher kinetic energies of impacting particles. On the other hand, the good correlation between the modelled transition velocity and the experimentally observed critical velocities suggests that attaining high strain rates due to shear instabilities is required only for a localised area to achieve successful bonding. A rough estimation shows that for impact velocities of 580 m/s, only about 15–25% of the entire interface is subject to shear instability. So far, the modelling has not been able to explain if this amount of surface area would be sufficient for a successful bonding. On the other hand, this could explain the relatively low bond strength of cold gas sprayed coatings as compared to bulk material or thermally sprayed coatings. Therefore, tensile tests could be used to supply additional information for assessing the extent of critical conditions at the interface. The bond strength of cold gas sprayed coatings, with particle velocities just exceeding critical velocity, are only about 20% of the ultimate tensile strength of bulk copper. This suggests that the ratio of surface area of the bonded interfaces to the total area should be about the same fraction. Taking into account the effect of stress concentrations at the edge of un-bonded areas, and contributions by shear due to impact morphologies, the results of tensile tests can be considered to be in good agreement with that of the modelling.

5.4. Open questions

The material properties used for the current analysis have been based on the data reported for bulk materials, and for strain rates which are by orders of magnitude smaller than those in cold gas spraying, in which strain rates can be in the range of 0.5×10^9/s per nanosecond. In addition, the current analysis does not take into account any phase changes in the material. Phase change could in particular influence the results of modelling for systems with allotropic transformations, such as for iron. Moreover, the properties of the feedstock powder may deviate substantially from those of bulk materials due to effects from high quenching rates and oxidation of powder during atomisation.

6. Conclusions

The present work demonstrates that plastic deformation phenomena in cold gas spraying can be modelled appropriately through finite element analysis. The results of the modelling provide a basis for understanding the bonding process. Based on these results, the bonding of particles can be attributed to adiabatic shear instabilities which occurs at the particle/substrate or particle/particle

interfaces at high velocities. The modelling also shows a very non-uniform development of strain and temperature at the interface, suggesting that this bonding is confined to a fraction of the interacting surfaces. This result is consistent with the relatively low strength of the copper coatings as determined experimentally. The analysis also suggests that density and particle temperature have significant effects on the critical velocity and are thus two of the most influential parameters in cold gas spraying. Overall, the analysis supplies a tool to predict critical velocities and to optimise spray parameters for different materials.

Acknowledgements

A part of this work was supported by Deutsche Forschungsgemeinschaft under grant No. KR1109/3-1. HA is grateful to GKSS and to the University of the Federal Armed Forces Hamburg for support throughout a visiting professorship.

Appendix A. Influences on critical velocities

The critical velocity, and its total differential, can be expressed as functions of process and material parameters $a_1,\ldots,a_n$ as follows

$$v_{cr} = f(a_1,a_2,\ldots,a_n) \tag{A.1}$$

$$dv_{cr} = \frac{\partial f}{\partial a_1}da_1 + \frac{\partial f}{\partial a_2}da_2 + \ldots + \frac{\partial f}{\partial a_n}da_n \tag{A.2}$$

Here, the maximum temperature at the interface, T_{max}, is taken as a key intermediate parameter. Assuming that a unique relationship exists between T_{max} and the process parameters, a translation formula can be used to give

$$\frac{\partial f}{\partial a_i} = -\frac{(\partial T_{max}/\partial a_i)}{(\partial T_{max}/\partial v)} \tag{A.3}$$

where v is the impact velocity. In a first approximation, these partial derivatives can be assumed to be process-independent constants. For small changes of parameters with respect to a reference condition, therefore, the critical velocity for the new condition can be obtained as

$$v_{cr} \approx v_{cr}^{ref} - \left(\frac{\partial v}{\partial T_{max}}\right)\left(\frac{\partial T_{max}}{\partial a_1}\Delta a_1 + \ldots + \frac{\partial T_{max}}{\partial a_n}\Delta a_n\right) \tag{A.4}$$

in which v_{cr}^{ref} is the critical velocity for the reference condition. By taking cold gas spraying of copper as the reference condition, for instance, the reference velocity shall take the value of 570 m/s. The partial derivatives of T_{max} on the right hand side of the above equation can be worked out numerically by calculating changes in T_{max} for small changes in the respective parameters. For instance, the change in T_{max} for 1 m/s increase in impact velocity has been found to be 1.3 K, over a wide range of impact velocity. The other derivatives were calculated in a similar manner with respect to parameters such as yield stress, density, melting temperature, and particle temperature.

References

[1] Herman H, Sampath S, McCune R. MRS Bull 2000;25:17.
[2] Fincke JR, Neiser RA. MRS Bull 2000;25:26.
[3] Kreye H, Gärtner F, Kirsten A, Schwetzke RH. High velocity oxy-fuel flame spraying state of the art, prospects and alternatives. In: Heinrich P, editor. Proceedings of the Fifth HVOF Colloquium. Unterschleißheim (Germany): Gemeinschaft Thermisches Spritzen; 2000. p. 5.
[4] Richter HJ. Fundamental thermodynamic and fluid dynamic concepts related to high velocity oxy-fuel spraying. In: Heinrich P, editor. Proceedings of the Fifth HVOF Colloquium. Unterschleißheim (Germany): Gemeinschaft Thermisches Spritzen; 2000. p. 4.
[5] Alkhimov AP, Kosareve VF, Papyrin AN. Dokl Akad Nauk SSSR 1990;315:1062.
[6] Alkhimov AP, Papyrin AN, Kosarev VF, Nesterovich NI, Shushpanov MM. Gas-dynamic spray method for applying a coating. US Patent 5,302,414; April 12, 1994.
[7] Alkhimov AP, Papyrin AN, Kosarev VF, Nesterovich NI, Shushpanov MM. Method and device for coating. European Patent 0 484 533 B1; January 25, 1995.
[8] McCune RC, Papyrin AN, Hall JN, Riggs II WL, Zajchowski PH. An exploration of the cold-gas-dynamic spray method for several materials systems. In: Berndt CC, Sampath S, editors. Advances in thermal spray science and technology. Materials Park (OH): ASM International; 1995. p. 1.
[9] McCune RC, Donlon WT, Cartwright EL, Papyrin AN, Rybicki EF, Shadley JR. Characterization of copper and steel coatings made by the cold-gas-dynamic spray method. In: Berndt CC, editor. Thermal spray: practical

solutions for engineering problems. Materials Park (OH): ASM International; 1996. p. 397.
[10] Dykhuizen RC, Smith MF. J Thermal Spray Tech 1998;7:205.
[11] Segall AE, Papyrin AN, Conway JC, Shapiro D. JOM 1998;9:52.
[12] Stoltenhoff T, Kreye H, Richter H. J Thermal Spray Tech 2002;11:542.
[13] Dykhuizen RC, Smith MF, Gilmore DL, Neiser RA, Jiang X, Sampath S. J Thermal Spray Tech 1999;8:559.
[14] Borchers C, Stoltenhoff T, Gärtner F, Kreye H, Assadi H. MRS Symp Proc 2001;673:P7.
[15] Papyrin AN, Kosarev VF, Klinkow SV, Alkhimov AP. On the interaction of high speed particles with a substrate under the cold spraying. In: Lugscheider EF, Berndt CC, editors. Proceedings of the International Thermal Spray Conference 2002. Düsseldorf (Germany): DVS-Verlag; 2002. p. 380.
[16] Brasher DG, Butler DJ. Adv Mater Process 1995;147:37.
[17] Murr LE, editor. Shock waves for industrial applications. New Jersey: Noyes Publications; 1988.
[18] Prümmer R. Explosivverdichtung pulvriger Substanzen: Grundlagen, Verfahren, Ergebnisse. Berlin: Springer, 1987.
[19] Deribas AA, Zakharenko ID. Fizika Goreniya i Vzryva 1974;10:409.
[20] Hammerschmidt M, Kreye H. Microstructure and bonding mechanism in explosive welding. In: Meyers MA, Murr LE, editors. Shock waves and high strain-rate phenomena in metals. New York: Plenum Press; 1981. p. 961.
[21] Zlobin SB, Pai VV, Yakovlev IV, Kuz'min GE. Combust Explosion Shock Waves 2000;36:256.
[22] Meyers MA, Thadhani NN, Yu LH. Explosive shock wave consolidation of metal and ceramic powder. In: Murr LE, editor. Shock waves for industrial applications. New Jersey: Noyes Publications; 1988. p. 265.
[23] Nesterenko VF. Dynamic loading of porous materials: potential and restrictions for novel materials applications. In: Murr LE, Staudhammer KP, Meyers MA, editors. Metallurgical and materials application of shock wave and high strain rate phenomena. Amsterdam: Elsevier; 1995. p. 3.
[24] Kasiray P, Vreeland T, Schwarz RB, Ahrens TJ. Acta Metall 1984;32:1235.
[25] Raybould D. J Mater Sci 1981;16:589.
[26] Staudhammer KP, Murr LE. Principles and applications of shock wave compaction and consolidation of powdered materials. In: Murr LE, editor. Shock waves for industrial applications. New Jersey: Noyes Publications; 1988. p. 237.
[27] Schwarz RB, Kasiraj P, Vreeland T, Ahrens TJ. Acta Metall 1984;32:1243.
[28] Rosato AD, Vreland T, Prinz FB. Int Mater Rev 1991;36:45.
[29] Gilmore DL, Dykhuizen RC, Neiser RA, Roemer TJ, Smith MF. J Thermal Spray Tech 1999;8:576.
[30] Papyrin A. Adv Mater Process 2001;159:49.
[31] ABAQUS™ 6.2-1. user manual. Hibbitt, Karlsson & Soerensen. Pawtucket (RI), 2001.
[32] Olson GB, Mescall JF, Azrin M. Adiabatic deformation and strain localization. In: Meyers MA, Murr LE, editors. Shock waves and high-strain-rate phenomena in metals. New York: Plenum Press; 1981. p. 22-1.
[33] Tzou DY. ASME J Heat Transfer 1995;117:8.
[34] Prakash GS, Reddy SS, Das SK, Sundararajan T, Seetharamu KN. Num Heat Transfer A 2000;38:513.
[35] Kapoor R, Nemat-Nasser S. Mech Mater 1998;28:1.
[36] Johnson GR. Prog Astronaut Aeronaut 1993;155:165.
[37] Karpp RR. Prog Astronaut Aeronaut 1993;155:223.
[38] Kamler F, Niessen P, Pick RJ. Can J Phys 1995;73:295.
[39] Nemat-Nasser S, Li Y. Acta Mater 1998;46:565.